Supplementary Information

Yue Wan[a], Xin Li[b], Xiaorui Wang[c], Xiaojun Yao[c], Benben Liao[a]*,
Chang-Yu Hsieh[a]*, Shengyu Zhang[a]*
[a] *Tencent Quantum Laboratory, Tencent, Shenzhen, PR China*
[b] *Department of Chemistry, Zhejiang University, Hangzhou, PR China*
[c] *State Key Laboratory of Quality Research in Chinese Medicines, Macau University of Science and Technology, Macao*

1 Transformer Explained

The core structure of vanilla Transformer [1] is the multi-head self attention. Attention, first introduced by Bahdanau et al. [2], is the mechanism where model could place different levels of attentiveness on each input element, just like human's cognitive attention on important terms when reading a sentence. It is essentially the mapping between a query vector and a set of key-value pairs. Multi-head attention is designated to use multiple attention functions on the same set of key-value pairs that allows model to attend to the information jointly from different dimensions. Each Transformer's encoder layer is composed of a multi-head self attention module and a feed forward (FFN) module. Layer normalization and residual connection is activated between each module. Let E^l_{in} and E^l_{out} be the encoder inputs and encoder outputs at l^{th} layer. Each layer of the encoder can be formulated as below:

$$\begin{aligned} E^l_{in} &= E^{l-1}_{out} \\ A &= \text{MultiHead}(E^l_{in}, E^l_{in}, E^l_{in}) \\ B &= \text{LayerNorm}(A + E^l_{in}) \\ C &= \text{FFN}(B) \\ E^l_{out} &= \text{LayerNorm}(C + B) \end{aligned} \tag{1}$$

Each Transformer's decoder layer is composed of a masked multi-head self attention module, a multi-head attention module that attends to the encoder outputs, and a FFN module. The masking within the multi-head self attention is applied to prevent the model from overlooking the future tokens while predicting the next token. Layer normalization and residual connection is also enforced. Let D^l_{in} and D^l_{out} be the decoder inputs and decoder outputs at l^{th} layer. Below is decoder's layer formulation:

$$\begin{aligned} D^l_{in} &= D^{l-1}_{out} \\ A &= \text{MaskedMultiHead}(D^l_{in}, D^l_{in}, D^l_{in}) \\ B &= \text{LayerNorm}(A + D^l_{in}) \\ C &= \text{MultiHead}(B, E^l_{out}, E^l_{out}) \\ D &= \text{LayerNorm}(C + B) \\ E &= \text{FFN}(D) \\ D^l_{out} &= \text{LayerNorm}(E + D) \end{aligned} \tag{2}$$

*Corresponding authors.
E-mail addresses: bliao@tencent.com (B. Liao), kimhsieh@tencent.com (C.-Y. Hsieh), shengyzhang@tencent.com (S. Zhang)

Table S1: Conditional template retrieval (GLN) and conditional template generation (Ours†) top-k accuracy given the ground truth reaction center.

Methods	*Top-k Accuracy(%)*				
	1	3	5	7	10
GLN	69.3	88.2	92.2	92.9	93.0
Ours†	72.5	91.0	94.2	95.1	95.9

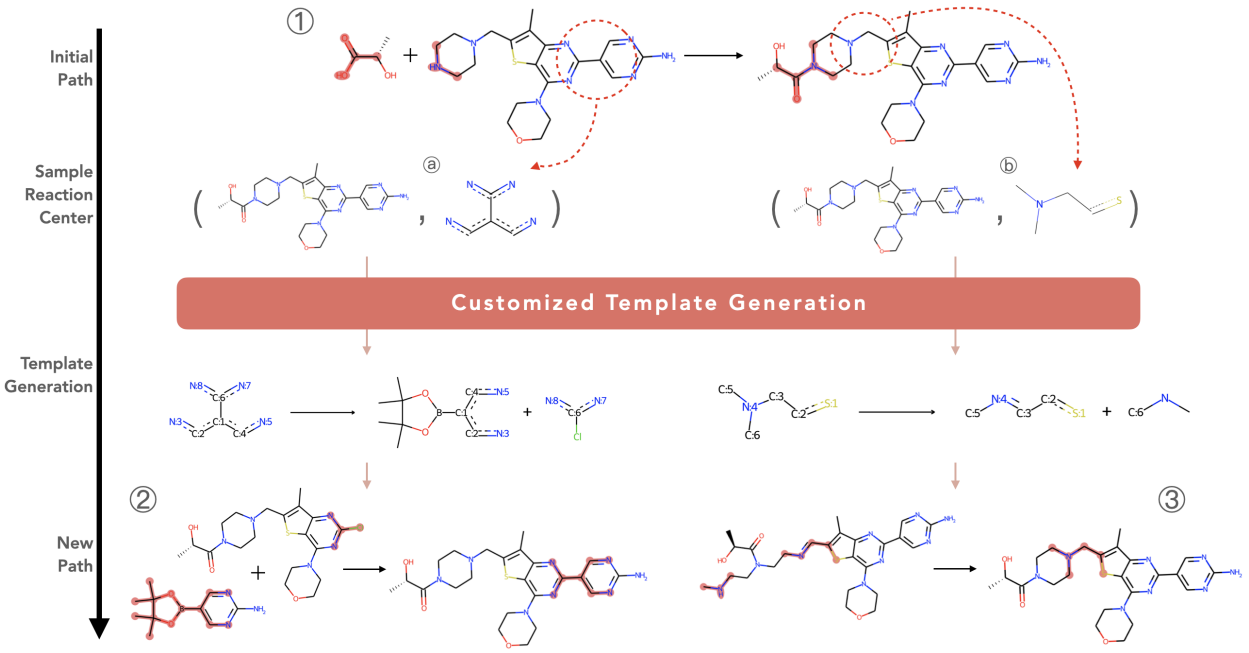

Figure S1: Template customization pipeline.

2 Template Generation versus Template Retrieval

We show in this section the detailed performance comparison between our approach and GLN's [3] template proposal (i.e. retrieval) module given the ground truth reaction center regarding to the top-k accuracy. For comparison purpose, we trained the reaction-class-known GLN model from scratch for 100 epoches using the same template format as we used, which is slightly more generalized than the default configuration of RDChiral [4]. We followed the default GLN's configuration for training. We then pulled out its conditional template proposal module and compared its top-k template accuracy with our methods with constraint $\hat{p} = p$ (Table S1). We could see, regarding to the top-k accuracy, our generative approach is as competitive as GLN's retrieval approach. It shows the promising potential for future researcher to develop a hybrid model that combines GLN with template generation for better synthesis planning performance.

3 Template Customization

Figure S1 is another example for the template customization pipeline. Here, we show multiple different synthetic pathways of Apitolisib [5, 6], which is an orally available agent with potential antineoplastic activity. By observation, we can easily identify multiple potential reaction centers of the molecule. Here we set reaction ①, a published path [7] which involves a peptide bond (highlighted in red), as the initial path that needs to be avoided. (a) and (b) are two of the randomly sampled reaction centers by our generative pipeline.

Table S2: AiZynthFinder's properties

Properties	Value
Exploratory parameter (UCT)	1.4
Cutoff cumulative	1
Cutoff number	50
Max transforms	6
Default prior	0.5
Use prior	True
Iteration limit	500
Return first	True
Time limit	500
Filter cutoff	0.05
Exclude target from stock	True
Prune cycles in search	True

Each of them is paired with the target product molecule and fed to the template generator. Reaction ② and ③ are two synthetic routes generated by the model. Reaction ② is the other documented route [8]. Its corresponding template already exists in USPTO-50K. It shows model's ability to retrieve knowledge from learned reaction space given a unseen molecule. Reaction ③ is an unpublished new candidate route, which is a simple ring-formation reaction. Its corresponding template does not exist in the training database, which indicates model's ability of inferring new chemical transformation.

4 Configuration of Multi-step Retrosynthesis Experiment

We used AiZynthFinder [9] as our evaluation multi-step retrosynthesis framework, which uses the Monte Carlo tree search algorithm over a precursor proposal systems. The detailed configuration for such algorithm is shown in Table S2.

5 Computational details

5.1 DFT Calculation

All DFT calculations were performed using Gaussian 16 software package [10]. Geometries optimization was conducted using DFT method M06-2X [11, 12] at the basis level of Def2SVP [13], including Grimme's D3 empirical dispersion corrections with zero-damping [14, 15]. To confirm whether each optimized stationary point is an energy minimum, as well as evaluate the zero-point vibrational energy and thermal corrections at 298 K, the vibrational frequencies were computed at the same level of theory as for the geometry optimizations. The single-point energies were computed at the M06-2X [11, 12] level of theory with the Def2TZVPP [13] basis set based on the gas-phase optimized structures [16, 17], with Grimme's D3 dispersion corrections [14, 15] as well. Considering the presence of carbocations, the solvation energies of methanol were evaluated by a self-consistent reaction field (SCRF) using the SMD model [18]. Extensive conformational searches for the intermediates have been conducted to ensure that the lowest energy conformers were located. In addition, to correct the Gibbs free energies under pressure of 1 atm to the standard state in solution (1 mol/L), a correction of $RT \ln (c_s/c_g)$ (about 1.89 kcal/mol) is added to energies of all species. c_s is the standard molar concentration in solution (1 mol/L), c_g is the standard molar concentration in gas phase (0.0446 mol/L), and R is the gas constant. A free energy correction of 4.3 kcal/mol for each species is also applied to further account for entropic effects in solution phase [19, 20, 21, 22, 23]. The Gibbs free energy difference of reaction

was evaluated as follows:

$$\Delta G_{rxn} = \sum G(products) - \sum G(reactants) + \Delta G_{gas-liquid} + \Delta G_{entropic} \quad (3)$$

5.2 Table of energies

Zero-point correction (ZPE), thermal correction to enthalpy (TCH), thermal correction to Gibbs free energy (TCG), energies (E), enthalpies (H), and Gibbs free energies (G) (in Hartree) of the structures for all the figures calculated at the M06-2X-D3/def2-TZVPP-SMD(methanol)// M06-2X-D3/def2-SVP level of theory.

Table S3: Energies for all calculated species

Structures	ZPE	TCH	TCG	E	H	G	Imaginary Frequency
P1	0.067314	0.074061	0.037348	-338.613681	-338.539620	-338.576333	–
P2	0.097528	0.103898	0.069553	-210.322900	-210.219002	-210.253347	–
R1	0.160400	0.171841	0.123750	-548.706539	-548.534698	-548.582789	–
R2	0.000000	0.002360	-0.010000	-0.213160	-0.210800	-0.223160	–

5.3 Cartesian coordinates of computed structures

P1

C	-0.22223200	-1.24341100	-0.00031700
C	-1.00751700	0.03001200	-0.00019300
C	0.94143900	1.22467000	-0.00007800
H	1.51868300	2.15465500	-0.00002000
N	-0.33965100	1.26095500	-0.00026700
O	-2.20962400	-0.04585600	0.00041700
C	1.18406600	-1.14067200	0.00015500
N	1.72771400	0.05321500	0.00027600
H	1.83952900	-2.01793000	0.00021500
H	-0.77219800	-2.19266000	-0.00099700

P2

N	0.51936700	-0.49781900	-0.32746600
C	1.64286400	0.35739100	0.00360400
H	1.40119900	1.39484300	-0.26607000
H	1.91219300	0.32824200	1.07376000
H	2.50619900	0.04038700	-0.59783600
C	-1.65080400	0.24146800	-0.18831200
H	-2.43000200	0.49445700	0.54274500
H	-1.41753200	1.13301000	-0.79433600
H	-2.02159400	-0.55124300	-0.85872200
O	-0.53709200	-0.18567800	0.54972400
H	0.75835400	-1.46269700	-0.09681900

R1

C	-2.06496400	0.94284100	0.43919600
C	-2.87278500	-0.72834100	-0.61264800
C	-1.51658100	-0.88802500	-0.67630200

N	-0.99236900	0.19092200	0.01793100
H	-1.91218500	1.86493600	0.99710900
H	-3.6 3658900	-1.36965800	-1.04615500
H	-0.88486300	-1.62211300	-1.16570500
N	-3.19696000	0.40900000	0.08935800
C	0.35988000	0.59002800	0.19760700
O	0.66090700	1.74638800	0.29216500
N	1.25358300	-0.46427000	0.15812600
C	1.07071300	-1.71133700	0.88468200
H	1.51420100	-2.53980700	0.31736600
H	1.57426200	-1.63203100	1.85940200
H	0.00552600	-1.90540100	1.04137600
C	3.08304000	0.35455900	-0.98069900
H	4.13978200	0.58410600	-0.80234100
H	2.99548500	-0.45035100	-1.72687000
H	2.56952100	1.26054900	-1.33550000
O	2.56775100	-0.05865600	0.26938400

R2

H	-3.34041579	1.43446146	0.00000000

References

[1] Vaswani, A. *et al.* Attention is all you need. In Guyon, I. *et al.* (eds.) *Advances in Neural Information Processing Systems*, vol. 30 (Curran Associates, Inc., 2017). URL https://proceedings.neurips.cc/paper/2017/file/3f5ee243547dee91fbd053c1c4a845aa-Paper.pdf.

[2] Bahdanau, D., Cho, K. & Bengio, Y. Neural machine translation by jointly learning to align and translate (2016). 1409.0473.

[3] Dai, H., Li, C., Coley, C., Dai, B. & Song, L. Retrosynthesis prediction with conditional graph logic network. In Wallach, H. *et al.* (eds.) *Advances in Neural Information Processing Systems*, vol. 32 (Curran Associates, Inc., 2019). URL https://proceedings.neurips.cc/paper/2019/file/0d2b2061826a5df3221116a5085a6052-Paper.pdf.

[4] Coley, C. W., Green, W. H. & Jensen, K. F. Rdchiral: An rdkit wrapper for handling stereochemistry in retrosynthetic template extraction and application. *Journal of Chemical Information and Modeling* **59**, 2529–2537 (2019). URL https://doi.org/10.1021/acs.jcim.9b00286. https://doi.org/10.1021/acs.jcim.9b00286.

[5] Aslan, O. *et al.* Preclinical evaluation and reverse phase protein array-based profiling of pi3k and mek inhibitors in endometrial carcinoma in vitro. *BMC Cancer* **18**, 168 (2018). URL https://doi.org/10.1186/s12885-018-4035-0.

[6] Ju, L. *et al.* Thieno [3,2-d] pyrimidine derivative containing indole structure and application thereof (Chinese Patent CN109879887A, Jun. 14 2019). URL https://patents.google.com/patent/CN109879887A.

[7] Sutherlin, D. P. *et al.* Discovery of a potent, selective, and orally available class i phosphatidylinositol 3-kinase (pi3k)/mammalian target of rapamycin (mtor) kinase inhibitor (gdc-0980) for the treatment of cancer. *Journal of Medicinal Chemistry* **54**, 7579–7587 (2011). URL https://doi.org/10.1021/jm2009327.

[8] Incorporated, G. *et al.* Combinations of phosphoinositide 3-kinase inhibitor compounds and chemotherapeutic agents and methods of use (Japanese Patent JP5658565B2, Jan. 28 2015). URL https://patents.google.com/patent/JP5658565B2.

[9] Genheden, S. *et al.* Aizynthfinder: a fast, robust and flexible open-source software for retrosynthetic planning. *Journal of Cheminformatics* 70 (2020).

[10] Frisch, M. J. *et al.* Gaussian˜16 Revision A.03 (2016). Gaussian Inc. Wallingford CT.

[11] Zhao, Y. & Truhlar, D. G. The m06 suite of density functionals for main group thermochemistry, thermochemical kinetics, noncovalent interactions, excited states, and transition elements: two new functionals and systematic testing of four m06-class functionals and 12 other functionals. *Theoretical Chemistry Accounts* **120**, 215–241 (2008). URL https://doi.org/10.1007/s00214-007-0310-x.

[12] Zhao, Y. & Truhlar, D. G. Density functionals with broad applicability in chemistry. *Accounts of Chemical Research* **41**, 157–167 (2008). URL https://doi.org/10.1021/ar700111a.

[13] Weigend, F. & Ahlrichs, R. Balanced basis sets of split valence, triple zeta valence and quadruple zeta valence quality for h to rn: Design and assessment of accuracy. *Phys. Chem. Chem. Phys.* **7**, 3297–3305 (2005). URL http://dx.doi.org/10.1039/B508541A.

[14] Grimme, S., Antony, J., Ehrlich, S. & Krieg, H. A consistent and accurate ab initio parametrization of density functional dispersion correction (dft-d) for the 94 elements h-pu. *The Journal of Chemical Physics* **132**, 154104 (2010). URL https://doi.org/10.1063/1.3382344. https://doi.org/10.1063/1.3382344.

[15] Grimme, S., Ehrlich, S. & Goerigk, L. Effect of the damping function in dispersion corrected density functional theory. *Journal of Computational Chemistry* **32**, 1456–1465 (2011). URL https://onlinelibrary.wiley.com/doi/abs/10.1002/jcc.21759. https://onlinelibrary.wiley.com/doi/pdf/10.1002/jcc.21759.

[16] Weigend, F. Accurate coulomb-fitting basis sets for h to rn. *Phys. Chem. Chem. Phys.* **8**, 1057–1065 (2006). URL http://dx.doi.org/10.1039/B515623H.

[17] Weigend, F. & Ahlrichs, R. Balanced basis sets of split valence, triple zeta valence and quadruple zeta valence quality for h to rn: Design and assessment of accuracy. *Phys. Chem. Chem. Phys.* **7**, 3297–3305 (2005). URL http://dx.doi.org/10.1039/B508541A.

[18] Marenich, A. V., Cramer, C. J. & Truhlar, D. G. Universal solvation model based on solute electron density and on a continuum model of the solvent defined by the bulk dielectric constant and atomic surface tensions. *The Journal of Physical Chemistry B* **113**, 6378–6396 (2009). URL https://doi.org/10.1021/jp810292n.

[19] Martin, R. L., Hay, P. J. & Pratt, L. R. Hydrolysis of ferric ion in water and conformational equilibrium. *The Journal of Physical Chemistry A* **102**, 3565–3573 (1998). URL https://doi.org/10.1021/jp980229p.

[20] Yu, Z.-X. & Houk, K. N. Intramolecular 1,3-dipolar ene reactions of nitrile oxides occur by stepwise 1,1-cycloaddition/retro-ene mechanisms. *Journal of the American Chemical Society* **125**, 13825–13830 (2003). URL https://doi.org/10.1021/ja0376487.

[21] Chen, Y. *et al.* Mechanistic twist of the [8+2] cycloadditions of dienylisobenzofurans and dimethyl acetylenedicarboxylate: stepwise [8+2] versus [4+2]/[1,5]-vinyl shift mechanisms revealed through a theoretical and experimental study. *Journal of the American Chemical Society* **129**, 10773–10784 (2007). URL https://doi.org/10.1021/ja072203u.

[22] Li, H., Wen, M. & Wang, Z.-X. Computational mechanistic study of the hydrogenation of carbonate to methanol catalyzed by the ruiipnn complex. *Inorganic Chemistry* **51**, 5716–5727 (2012). URL https://doi.org/10.1021/ic300175b.

[23] Yu, J.-L., Zhang, S.-Q. & Hong, X. Mechanisms and origins of chemo- and regioselectivities of ru(ii)-catalyzed decarboxylative c–h alkenylation of aryl carboxylic acids with alkynes: A computational study. *Journal of the American Chemical Society* **139**, 7224–7243 (2017). URL https://doi.org/10.1021/jacs.7b00714.